Semiconductivity and High Stability in Centimetric Two-Dimensional Bismuth-Silver Hybrid Double Perovskites

Mohamed Saber Lassoued,[a] Tengbo Wang,[b] Qian-Wen Li,[a] Xiaoyun Liu,[c,d] Wei-Peng Chen,[a] Bo Jiao,[c,d] Qing-Yuan Yang,[e] Zhaoxin Wu,[c,d] Guijiang Zhou,[a] Shujiang Ding,[a] Zhicheng Zhang,[a] and Yan-Zhen Zheng*[a]

---

[a] School of Chemistry, State Key Laboratory for Mechanical Behavior of Materials, MOE Key Laboratory for Nonequilibrium Synthesis and Modulation of Condensed Matter, Xi'an Jiaotong University, Xi'an 710049 China.
E-mail : ***zheng.yanzhen@xjtu.edu.cn***

[b] School of Automation Science and Technology, No. 4 Building, Xi'an Jiaotong University, Siyuanhuan North Road, Xi'an, Shaanxi, China.

[c] Key Laboratory of Photonics Technology for Information, Key Laboratory for Physical Electronics and Devices of the Ministry of Education, Department of Electronic Science and Technology, School of Electronic and Information Engineering, Xi'an Jiaotong University, Xi'an, China.

[d] Collaborative Innovation Center of Extreme Optics, Shanxi University, Taiyuan 030006, China.

[e] School of Chemical Engineering and Technology, Xi'an Jiaotong University, Xi'an 710049, China.

Table of content

1. General remarks

Single crystal X-ray diffraction data of ABB-1 and ABB-2 were collected on a Bruker SMART APEX II CCD diffractometer with graphite monochromated Mo-k radiation (λ= 0.71073 Å) by using the θ-ω scan technique at 150 K. PXRD intensities were measured at ambient temperature (298 K) on a Rigaku D/max-IIIA diffractometer (Cu-kλ, λ=1.54056 Å). The crystalline powder samples were prepared by grinding the single-crystals and collected in the 2θ range of [5°–50°] with a step size of 5°/min at room temperature. Scanning electron microscopy (SEM) was performed using KYKY-EM3200, 25 KV instrument. Solid-state UV-Vis diffusion reflectance spectra of pressed powder and films samples were measured on a SHIMADZU UV-3600 UV-Vis-NIR spectrophotometer using $BaSO_4$ powder as the reflectance reference. All density-functional theory (DFT) calculations were carried out within CASTEP software. Room-temperature steady-state emission spectra were collected on powder samples using an Edinburgh FLS985 fluorimeter upon 365 nm excitation.

2. Materials and Sample Preparation

2.1. Materials

Chemicals listed were used as purchased and without further purification: (i) 1-ethylpiperazine (EPZ), 99.5%, sigma Aldrich; (ii) 1-methylpiperidin-4-amine (MPA), 97%, sigma Aldrich; (iii) Bismuth oxide, 9.995%, sigma Aldrich; (iii) Silver oxide, 99%, sigma Aldrich; (iv) hydrobromic acid, 48% w/w, sigma Aldrich.

2.2. Preparation of ABB-1 and ABB-2 Single crystals

Crystals of ABB-1: A mixture of Bi_2O_3 (0.465 g, 1 mmol), Ag_2O (0.231 g, 1 mmol) and EPZ (0.114 g, 1 mmol) were dissolved in 10ml HBr, stirred in the air for 10 minutes before transferred to a 15 mL Teflon-lined auto-clave and heated at 120°C for 6 hrs. The reactants were then cooled to room temperature in a rate of 5°C / h to obtain Luminous light-yellow needle-like crystals. (Yield: ca. 60% based on Bi). XRD indicates the phase purity (**Figure S3 (a)**).

Crystals of ABB-2: A mixture of Bi_2O_3 (0.465 g, 1 mmol), Ag_2O (0.231 g, 1 mmol)

and AMP (0.114 g, 1 mmol) were dissolved in 10ml HBr, stirred in the air for 10 minutes before transferred to a 15 mL Teflon-lined auto-clave and heated at 120°C for 6 hrs. The reactants were then cooled to room temperature in a rate of 5 °C / h to obtain Luminous transparent rod-like crystals. (Yield: ca. 62% based on Bi). XRD indicates the phase purity (**Figure S3 (b)**).

2.3. Fabrication of ABB-1 and ABB-2 Films

Indium tin oxide coated glass (ITO) substrates were cleaned thoroughly and sequentially with commercial detergent in soapy water, deionized water, KOH solution, deionized water, and in a sonication bath. The substrates were then treated by UV–ozone treatment for 20 min prior before use. ABB-1 and ABB-2 organic-inorganic hybrid compounds (0.2 g for each compound) were dissolved in 1 mL of dimethyl sulfoxide solution (DMSO) and were coated onto ITO glass substrate by spin coating method at 1000 rpm for 60 second. To evaporate the residual solvent, the obtained film was followed by annealing on a hot plate at 80 °C for 10 minutes.

3. Characterization methods and Simulation details

3.1. Characterization methods

X-ray Crystallographic Study. Single-crystal X-ray diffraction data collections for ABB-1 and ABB-2 were conducted on a Bruker SMART APEX II CCD diffractometer (Mo, λ = 0.71073 Å) by using the θ-ω scan technique at 150 K. The structures were solved by direct methods and refined with a full-matrix least-squares technique within the SHELXTL program package. [S1] All non-hydrogen atoms were refined anisotropically. The crystallographic details are provided in **Table S1-S5**. Crystallographic data for the structural analyses has been deposited at the Inorganic Crystal Structure Database. CCDC number of ABB-1 and ABB-2 are 2150677, 2150680 respectively. The crystallographic data for above compounds can be found in the Supporting Information or can be obtained free of charge from the Inorganic Crystal Structure Database via http://www.ccdc.cam.ac.uk/data_request/cif.

Optical absorption measurement. Solid-state UV-Vis diffusion reflectance spectra were measured at ambient temperature on a SHIMADZU UV-3600 UV-Vis-NIR spectrophotometer using $BaSO_4$ powder as the reflectance reference. The absorption spectra were calculated from reflectance spectra by the Kubelka-Munk function: $F(R) = \alpha/S = (1-R)^2/2R$, where R, α, and S are the coefficients for the reflection, the absorption and the scattering, respectively.

Photoluminescence measurement. Room-temperature steady-state emission spectra were collected on powder samples using an Edinburgh FLS985 fluorimeter upon 365 nm excitation. Due to the weak emission spectra were affected by noise, 400 nm filter was used to reduce the noise.

Stability studies.

Freshly prepared Perovskites films of ABB-1 and ABB-2 were deposited on clear plate glasses and thereafter they were placed inside sealed jar containing a saturated solution of $Mg(NO_3)_2.6H_2O$, stored either in the dark to minimize light exposure and the relative humidity was maintained at ~55% humidity. [S2] The films were not in direct contact with the solution and were periodically analyzed with PXRD.

Photocurrent measurements. The pellets were prepared by grinding 50-100 mg polycrystalline samples of ABB-1 and ABB-2 into a homogeneous powder after pressed with 15 MPa for 10 minutes. Each pellet was connected to two wires at one side (up or down) using conductive silver paste. It's worthy to note that we left one narrow strip like area without paint which can receive light from the lamp. A 350 W solar-simulating Xenon lamp was used as light source. For each 80 s we past or blocked the light and detected the current change.

Proton Conductivity measurements. Proton conductivity determination was based on quasi-four-electrode AC impedance technique with Solatron SI 1260 Impedance/Gain phase Analyzer over a frequency range from 1 Hz to 1 MHz and the amplitude of 50 mV. The pellets of 8.00 mm in diameter and ~1 mm in thickness were prepared by grinding 80 mg polycrystalline samples of ABB-1 and

ABB-2. The pellets were then coated with silver paste on both sides and connected to Pt wires. The proton conductivity (σ) is calculated by the equation $R = \rho d/A = d/(\sigma A)$ and thus $\sigma = d/(RA)$ where R is the charge resistance of proton transport, σ is the proton conductivity, ρ is the electrical resistivity equals to $1/\sigma$, d is the measurement length of the conductor and A is the cross-section area of the conductor. Activation energy (Ea) of proton conductivity (σ) was extracted from the data measured at various temperatures (95% RH) by using the Arrhenius equation: $\sigma = (\sigma_0/T)\cdot\exp[-Ea/(k\cdot T)]$, where σ_0, T and k is the pre-exponential factor, temperature and Boltzmann constant, respectively.

3.2 Simulation details Computational methods.

The crystallographic data of compound ABB-1 and ABB-2 obtained from Single Crystal XRD tests were used to calculate the electronic band structures and partial densities of the states (PDOS). All the calculations in this work were carried out using density functional theory (DFT) as implemented in the BIOVIA Materials Studio Simulation Package. [S3, S4] The generalized gradient approximation (GGA) Perdew–Burke–Ernzerhof (PBE) functional was used for electronic structure calculations. [S5] The convergence threshold for the self-consistent field was 2×10^{-6} eV/atom. The pseudopotential form was OTFG ultrasoft mode and the energy cutoff was 489.8 eV. The DFT calculation of ABB-1 and ABB-2 band structure were executed with or without SOC in an elastic compute servicer with 24 cores and 96 GB memory. When excluding the spin orbit coupling (SOC), the kinetic energy cutoff we used was 260 eV with ultrasoft pseudopotentials. For the case of including the SOC, we applied norm conserving pseudopotentials and the kinetic energy cutoff was 600 eV.

4. Supporting Tables and Figures

Table S1 Crystal data and structure refinement for compound ABB-1 and ABB-2

	ABB-1	**ABB-2**
Empirical formula	C_{12} H_{32} Ag Bi Br_8 N_4	C_{12} H_{32} Ag Bi Br_8 N_4
Formula weight	1188.47	1188.47
Crystal dimensions (mm)	0.1*0.24*0.16	0.11*0.17*0.12
Crystal system	Monoclinic	Monoclinic
Space group	$P2_1/c$	$P2_1/n$
a/Å	8.191(4)	7.9857(19)
b/Å	9.537(4)	9.403(2)
c/Å	17.937(8)	18.518(5)
α/°	90	90
β/°	103.2000	99.938(3)
γ/°	90	90
Volume/Å^3	1364.2(11)	1369.6(6)
Z	2	2
ρ calcg/cm^3	2.893	2.882
μ /mm^{-1}	18.882	18.808
F(000)	1084.0	1084.0
Index ranges	-10<=h<=10, -12<=k<=12, -23<=l<=23	-9<=h<=9, -11<=k<=11, -23<=l<=23
Data Completeness	93.9%	99.1%
Data/restraints/parameters	3350/0/122	2867/0/121
Goodness-of-fit on F2	1.11	1.11
Weight	$w = 1/[\sigma^2(Fo^2) + (0.0493P)^2 + 11.6237P]$ where $P = (Fo^2 + 2Fc^2)/3$	$w = 1/[\sigma^2(Fo^2) + (0.0238P)^2 + 5.4014P]$ where $P = (Fo^2 + 2Fc^2)/3$
$R=\sum\|\|Fo-Fc\|\|/\sum\|Fo\|$, wR_2	$R_1 = 0.046$, $wR_2 = 0.139$	R1 = 0.029, wR2 = 0.069

$R1 = \Sigma||Fo| - |Fc||/\Sigma|Fo|$, $wR_2 = [\Sigma w(Fo^2 - Fc^2)^2 / \Sigma w(Fo^2)^2]^{1/2}$

Table S2 Summary of selected bond lengths (Å) and bond angles (°) of ABB-1

Bond	Lengths/Å	Bond pair	Angles / °	Bond pair	Angles / °
Ag1-Br3	3.4623 (15)	Br4^{ii}-Ag1-Br4	180.00 (4)	C1-N2-C4	109.05 (7)
Ag1-Br4	2.5039 (14)	Br3-Ag1- Br4	85.75 (3)	C5-N2-C4	110.75 (7)
Ag1-Br4^{ii}	2.5039 (14)	Br3-Ag1- Br4^{ii}	94.25 (3)	C5-N2-C1	113.12 (7)
Bi1-Br3^{i}	2.8669 (13)	Br3-Bi1-Br3^{i}	180	C1-C2-N1	110.93 (7)
Bi1-Br3	2.8668 (13)	Br1^{i}-Bi1-Br3^{i}	93.45 (3)		
Bi1-Br1^{i}	2.8648 (15)	Br1^{i}-Bi1-Br3	86.55 (3)		
Bi1-Br1	2.8648 (15)	Br1-Bi1-Br3^{i}	86.55 (3)		
Bi1-Br2	2.8578 (12)	Br1-Bi1-Br3	93.45 (3)		
Bi1-Br2^{i}	2.8578 (12)	Br1-Bi1-Br1^{i}	180		
N1-C3	1.5039 (11)	Br2^{i}-Bi1-Br3	94.81 (4)		
N2-C4	1.5022 (11)	Br2^{i}-Bi1-Br3^{i}	85.19 (4)		
N2-C1	1.5060 (12)	Br2-Bi1-Br3	85.19 (4)		
N2-C5	1.5318 (11)	Br2-Bi1-Br3^{i}	94.81 (4)		
C2-C1	1.5351 (12)	Br2^{i}-Bi1-Br1^{i}	91.79 (3)		
C5-N2	1.5318 (11)	Br2-Bi1-Br1^{i}	88.21 (3)		
C5-C6	1.5345 (15)	Br2-Bi1-Br1	91.79 (3)		
C3-N1	1.5039 (12)	Br2^{i}-Bi1-Br1	88.21 (3)		
C3-C4	1.5138 (12)	Br2-Bi1-Br2^{i}	180		
C1-N2	1.5060 (12)	Bi1-Br3-Ag1	166.53 (3)		
C1-C2	1.5351 (12)	C3-N1-C2	112.28 (7)		
C4-N2	1.5022 (11)	C2-C1-N2	111.34 (7)		
C4-C3	1.5138 (12)	C4-C3-N1	110.19 (7)		
C6-C5	1.5345 (15)	C3-C4-N2	111.03 (7)		
N1-C2	1.4681 (12)	C6-C5-N2	111.20 (8)		

Symmetry codes: (i) −x+1, −y+1, −z+1; (ii) −x, −y+2, −z+1.

Table S3 Summary of selected bond lengths (Å) and bond angles (°) of ABB-2

Bond	Lengths/Å	Bond pair	Angles / °	Bond pair	Angles / °
Bi1-Br2^{i}	2.8753 (9)	Br1^{i}-Bi1-Br1	85.52 (4)	C2-C3 -C4	110.79 (6)
Bi1-Br1	2.8293 (8)	Br2^{i}-Bi1-Br1	92.22 (2)	C5-C6-N2	111.40 (5)
Bi1-Br1^{i}	2.8294 (8)	Br2-Bi1-Br1	91.19 (2)	C6-C5-C4	108.79 (6)
Bi1-Br2	2.8753 (9)	Br3^{i}-Bi1-Br1	88.67 (3)	C3-C2 -N2	110.01 (5)
Bi1-Br3^{i}	2.8920 (8)	Br3-Bi1-Br1	173.77 (2)	C5-C4-N1	108.87 (6)
Bi1-Br3	2.8920 (8)	Br2^{i}-Bi1-Br1^{i}	91.19 (2)	C5-C4-C3	110.54 (6)
Ag1-Br4	2.5403 (9)	Br2-Bi1-Br1^{i}	92.22 (2)	C2-N2 -C6	110.65 (5)
Ag1-Br4^{ii}	2.5403 (9)	Br3^{i}-Bi1-Br1^{i}	173.77 (2)		
Ag1-Br3	3.2306 (13)	Br3-Bi1-Br1^{i}	88.67 (3)		
N1-C4	1.4846 (8)	Br2-Bi1-Br2^{i}	175.36 (3)		
N2-C1	1.4740 (8)	Br3^{i}-Bi1-Br2^{i}	91.29 (2)		
N2-C6	1.4770 (9)	Br3-Bi1-Br2^{i}	85.64 (2)		
N2-C2	1.4963 (8)	Br3^{i}-Bi1-Br2	85.64 (2)		
C4-N1	1.4846 (8)	Br3-Bi1-Br2	91.29 (2)		
C4-C3	1.5141 (9)	Br3-Bi1-Br3^{i}	97.21 (3)		
C4-C5	1.5277 (9)	Br4^{ii}-Ag1 -Br4	160.17 (6)		
C3-C2	1.5325 (9)	Br3-Ag1 -Br4	96.25 (3)		
C6-N2	1.4770 (9)	Br3-Ag1 -Br4^{ii}	100.03 (3)		
C6-C5	1.5434 (10)	Ag1-Br3-Bi1	164.45 (3)		
C5-C4	1.5277 (9)	C6-N2 -C1	111.51 (6)		
C2-N2	1.4963 (8)	C2-N2 -C1	110.56 (5)		
C2-C3	1.5325 (9)	H2-N2 -C1	107.99		
C1-N2	1.4740 (8)	C3-C4-N1	110.02 (6)		

Symmetry codes: (i) −x+3/2, y, −z+3/2; (ii) −x+1/2, y, -z+3/2.

Table S4 Potential hydrogen bonding data of compound ABB-1

D-H	d(D-H)	d(H..A)	<DHA	d(D..A)	A	
N1-H1A	0.89	2.861	135.31	3.55	Br3	[x, -y+3/2, z-1/2]
N1-H1A	0.89	2.748	135.88	3.443	Br2	[x, -y+3/2, z-1/2]
N1-H1B	0.89	2.732	138.4	3.449	Br3	[-x, y+1/2, -z+1/2]
N1-H1B	0.89	3.058	121.25	3.601	Br1	[x-1, -y+3/2, z-1/2]
N1-H1B	0.89	3.065	128.41	3.685	Br2	[-x, y+1/2, -z+1/2]
N2-H2	0.98	2.353	166.89	3.315	Br4	
C2-H2A	0.97	3.055	135.54	3.808	Br4	
C2-H2B	0.97	2.776	151.85	3.659	Br4	[-x, y+1/2, -z+1/2]
C2-H2B	0.97	3.011	117.4	3.563	Br2	[x, -y+3/2, z-1/2]
C5-H5A	0.97	2.944	149.58	3.813	Br1	[x, -y+3/2, z-1/2]
C3-H3A	0.97	3.075	116.93	3.62	Br3	[x, -y+3/2, z-1/2]
C3-H3A	0.97	2.8	129.78	3.501	Br4	[-x, y-1/2, -z+1/2]
C3-H3B	0.97	2.981	129.26	3.673	Br1	[x-1, -y+3/2, z-1/2]
C1-H1C	0.97	2.934	150.34	3.807	Br1	[x, -y+3/2, z-1/2]
C4-H4B	0.97	3.037	146.82	3.885	Br1	[x, -y+3/2, z-1/2]

Table S5 Potential hydrogen bonding data of compound ABB-2

D-H	d(D-H)	d(H..A)	<DHA	d(D..A)	A	
N1-H1A	0.89	2.915	138.83	3.633	Br3	[-x, -y+1, -z+1]
N1-H1A	0.89	2.846	138.63	3.563	Br3	[x-1/2, -y+1, z-1/2]
N1-H1B	0.89	2.756	131	3.407	Br1	[x-3/2, -y+1, z-1/2]
N1-H1C	0.89	2.546	166.33	3.417	Br2	[-x+1, -y+1, -z+1]
N2-H2	0.98	2.326	174.21	3.303	Br4	
C4-H4	0.98	2.904	159.32	3.837	Br2	[-x, -y+1, -z+1]
C3-H3B	0.97	3.125	139.64	3.915	Br4	[-x, -y, -z+1]
C6-H6A	0.97	2.949	152	3.833	Br2	[x-1, y, z]
C5-H5A	0.97	2.989	140.44	3.788	Br4	[-x, -y+1, -z+1]
C2-H2B	0.97	2.87	134.27	3.615	Br2	[x-1, y-1, z]
C1-H1D	0.96	3.029	153.01	3.909	Br3	[-x+1/2, y, -z+3/2]

Table S6 Distortion degree of M^I coordination geometries for different bimetallic hybrid perovskites.

Compounds	Organic ligand	Δd (M^I)	References
$C_{12}H_{34}BiCuI_8N_4O$	Cyclohexane-1,4-diamine	0.171	[S6]
$C_{27}H_{62}BiCuI_8N_4$	Cyclohexylamine	0.167	[S6]
$C_{32}H_{72}BiCuI_8N_4$	Cyclooctylamine	0.1812	[S6]
$C_{50}H_{120}Bi_3CuI_{20}N_1$	Cyclopentylamine	0.148	[S7]
$C_{35}H_{84}Bi_2CuI_{14}N_7$	Cyclopentylamine	0.174	[S6]
$C_{12}H_{34}AgBiI_8N_4O$	Cyclohexane-1,4-diamine	0.147	[S7]
$C_{12}H_{32}AgBiBr_8N_4$	1-ethylpiperazine	0.138	This Work
$C_{12}H_{32}AgBiBr_8N_4$	1-methylpiperidin-4-amine	0.116	This Work

Table S7. Photoelectric properties comparison of ABB-1 and ABB-2 with other reported halide hybrid perovskite materials

Compounds	Dimensionality	Voltage applied (V)	I_{light} (nA)	I_{dark} (nA)	I_{light}/I_{dark}	Device	Ref
ABB-1	2D	7	15.34	0.16	95.87	Pellet	This work
ABB-2	2D	7	16.14	0.18	89.66	Pellet	This work
$(C_6H_{13}N)_2BiI_5$	1D	10	7.35	2.5	2.94	Film	[S8]
$(C_{12}H_{30}N_4)Cs_3BiI_8$	2D	11	21.51	4.81	4.47	Pellet	[S9]
$(C_3H_{12}N_2)_2Bi_2I_{10}.2H_2O$	0D	1	194	94	2.1	Film	[S10]
$(C_6H_{16}N_2)_2AgBiI_8.H_2O$	2D	40	7.92	0.184	44.2	Pellet	[S11]
$(C_6H_{14}N)_4CuBiI_8$	2D	3	20	2.5	8	Pellet	[S6]
$(C_5H_7N_2)BiI_4$	1D	10	0.25	0.02	12.5	Crystal	[S12]
$(s\text{-}BA)_2\ (MA)Pb_2I_7$	2D	10	35.97	0.07	513.85	Crystal	[S13]
$(4\text{-}TFBMA)_2(DMA)Pb_2I_7$	2D	10	56.7	0.096	590.625	Crystal	[S14]
$[Fe(bipy)_3]AgBiI_6$	0D	-	150	60	2.5	powder	[S15]

s-BA: Sec-butylammonium / MA: methylammonium / 4-TFBMA: 4-(trifluoromethyl) benzylammonium / DMA: dimethylammonium / bipy: 2,2′- bipyridine

Table S8. Stability tests comparison of ABB-1 and ABB-2 with other reported Pb-free halide perovskite materials

Compounds	Test period (d)	Test condition	Stability	Ref
$Cs_3Bi_2I_9$	30	<10% RH	Stable	[S16]
$AgBi_2I7$	10	/	Stable	[S17]
$MA_3Bi_2I_9$	25	61% RH	Stable	[S18]
$C_5H_6NBiI_4$	7	/	Stable	[S19]
Cs_2NaBiI_6	150	70% RH	Stable	[S20]
$(C_6H_{16}N_2)_2BiAgI_8 \cdot H_2O$	30	55% RH	Stable	[S7]
$(C_6H_{16}N_2)_2CuBiI_8 \cdot 0.5H_2O$	30	55% RH	Stable	[S7]
$(C_{10}H_{26}N_4)_2BiAgI_8.H_2O$	30	55% RH	Stable	[S21]
ABB-1	90	55% RH	Stable	This work
ABB-2	90	55% RH	Stable	This work

Table S9. Proton conductivities comparison of ABB-1 and ABB-2 with other reported related crystalline materials

Compounds	Measurement conditions	σ(S cm^{-1})	Ref
[$PbCl_2$(HOOCMMIm)]	75 °C, 98%RH	6.53 × 10^{-2}	[S22]
[$PbBr_2$(HOOCMMIm)]	75 °C, 98%RH	3.54 × 10^{-3}	[S22]
Triethylpropylammonium[PbI_3]	200 °C, 0% RH	4.47 × 10^{-5}	[S23]
Co_3(p-ClPnHIDC)$_3$(H_2O)$_3$]·6H_2O}n	100 °C, 93%RH	1.47 × 10^{-4}	[S24]
[Cu_2(Htzehp)$_2$(4,4′-bipy)]·3H_2O	95 °C, 80%RH	1.43 × 10^{-3}	[S25]
$C_{11}H_9ClN_2O_4Zn$	100 °C, 98%RH	4.72 × 10^{-3}	[S26]
ABB-1	95 °C, 95%RH	7.96 × 10^{-4}	This work
ABB-2	95 °C, 95%RH	9.83 × 10^{-4}	This work

.

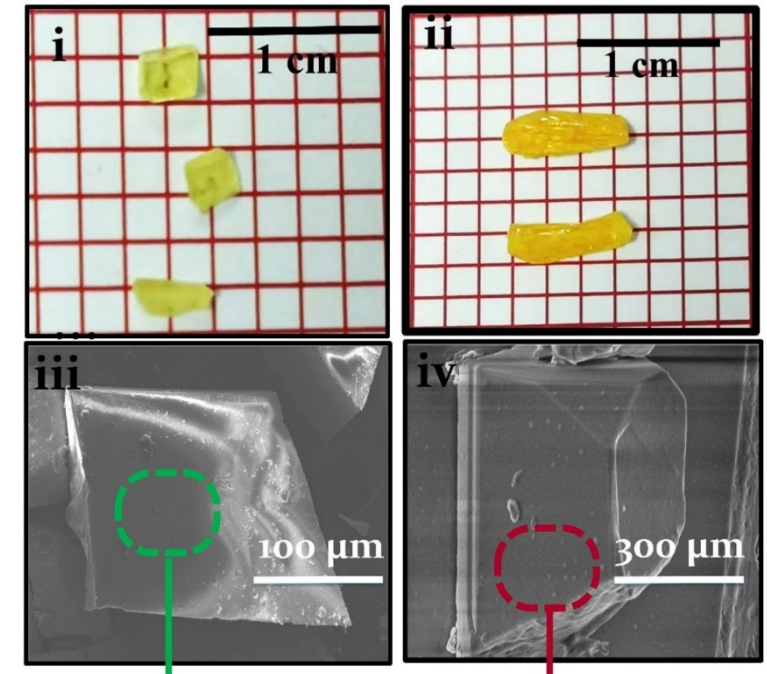

v

Element (atom %)	Ag	Bi	Br
(ABB-1)	10.54	8.89	80.57
(ABB-2)	10.41	9.45	80.14

Figure S1. Photographs of the obtained SCs of ABB-1 (i) and ABB-2 (ii). SEM images of ABB-1 (iii) and ABB-2 (iv). EDS elemental analysis results of ABB-1 and ABB-2 (v).

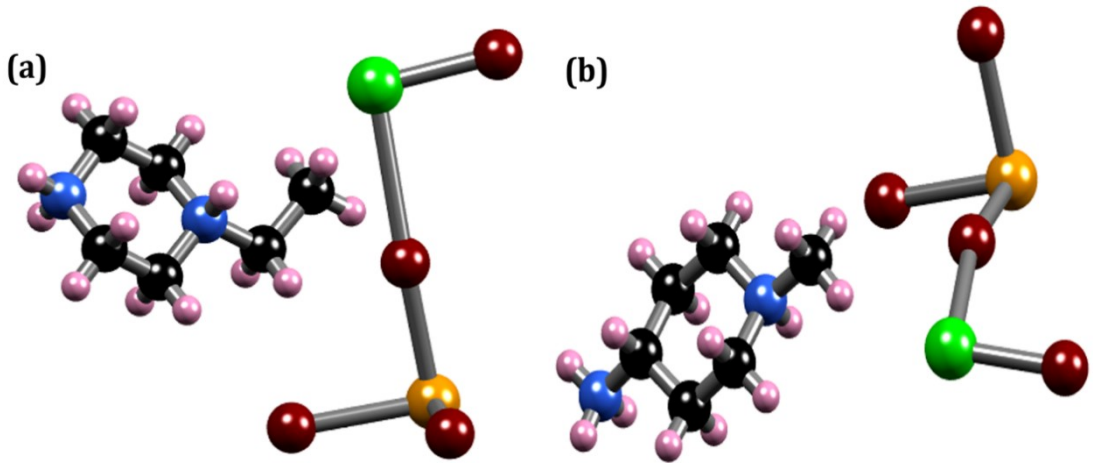

Figure S2. (a) Assymetric unit for ABB-1. (b) Assymetric unit for ABB-2. The colors are used to indicate the following: Bismuth: orange, Silver: light green, bromine: brown, Carbon: black, Nitrogen: blue and Hydrogen: pink

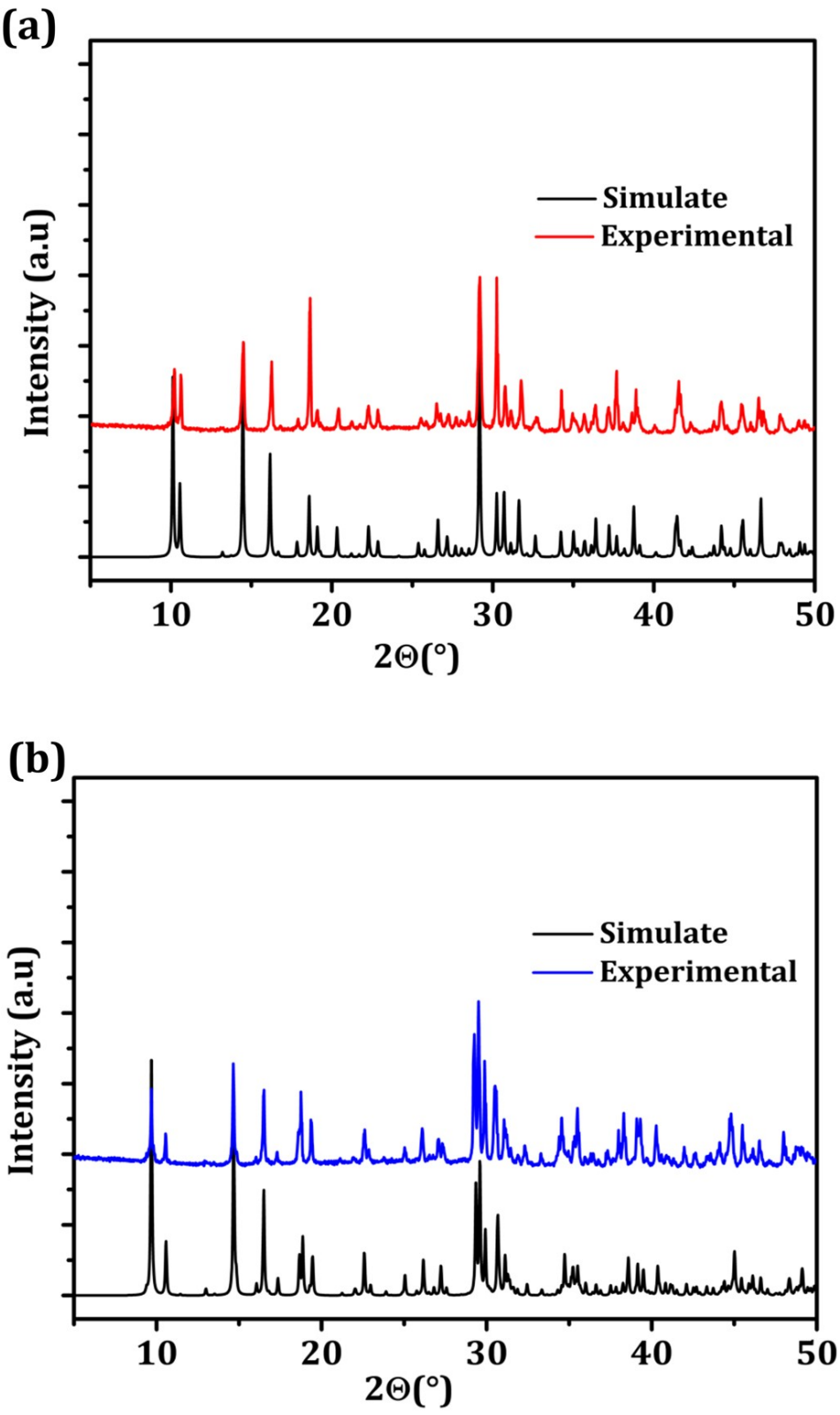

Figure S3. (a) Powder XRD patterns for ABB-1. (b) Powder XRD patterns for ABB-2.

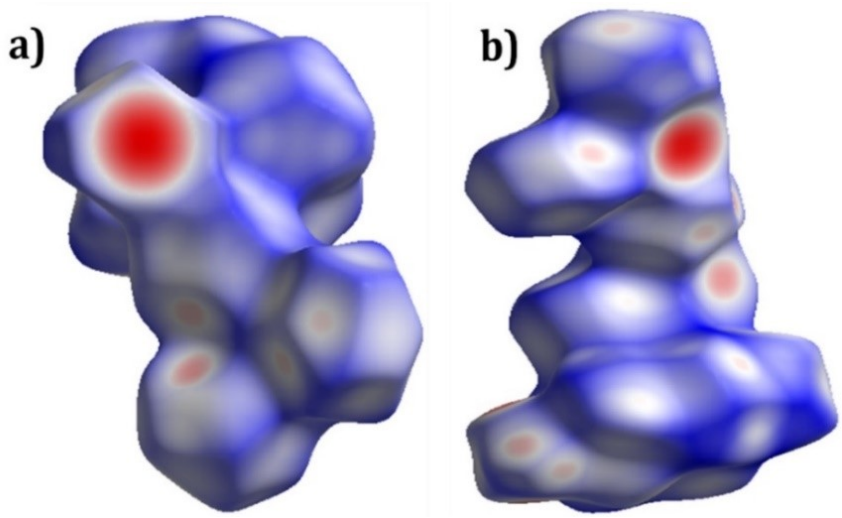

Figure S4. Hirshfeld surfaces mapped with dnorm ABB-1 (a) and ABB-2 (b) (color coding: white, distance d equals VDW distance; blue, d exceeds VDW distance, red, d, smaller than VDW distance)

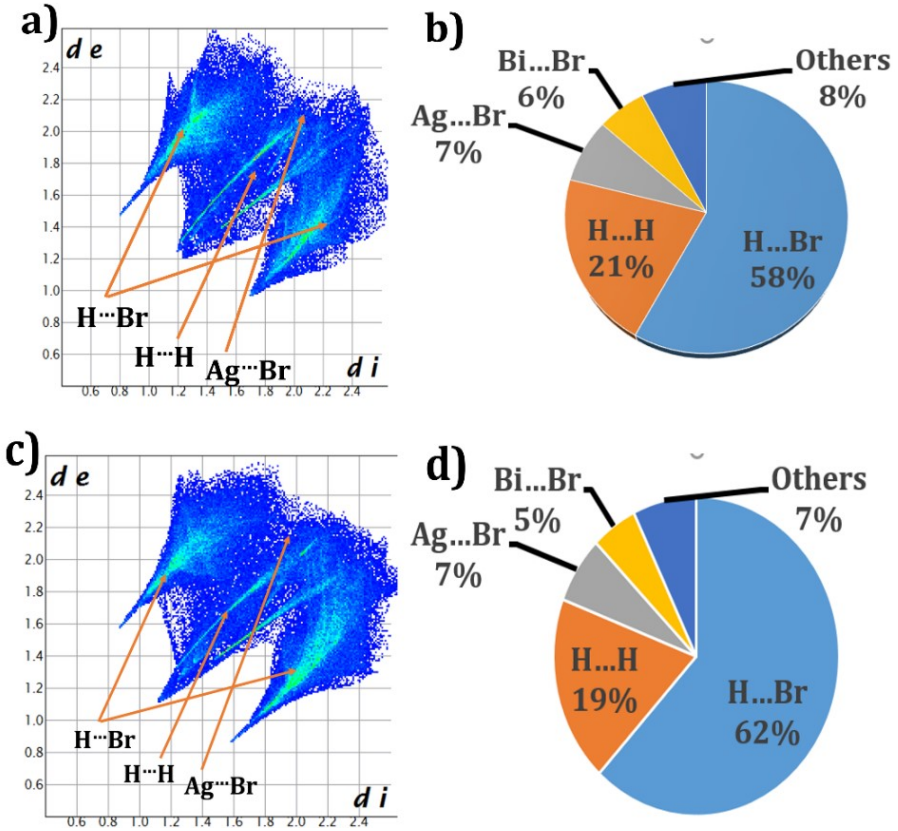

Figure S5. Two-dimensional finger print plots for ABB-1 (a) and ABB-2 (c). The population of close contact for ABB-1 (b) and ABB-2 (d) in crystal stacking.

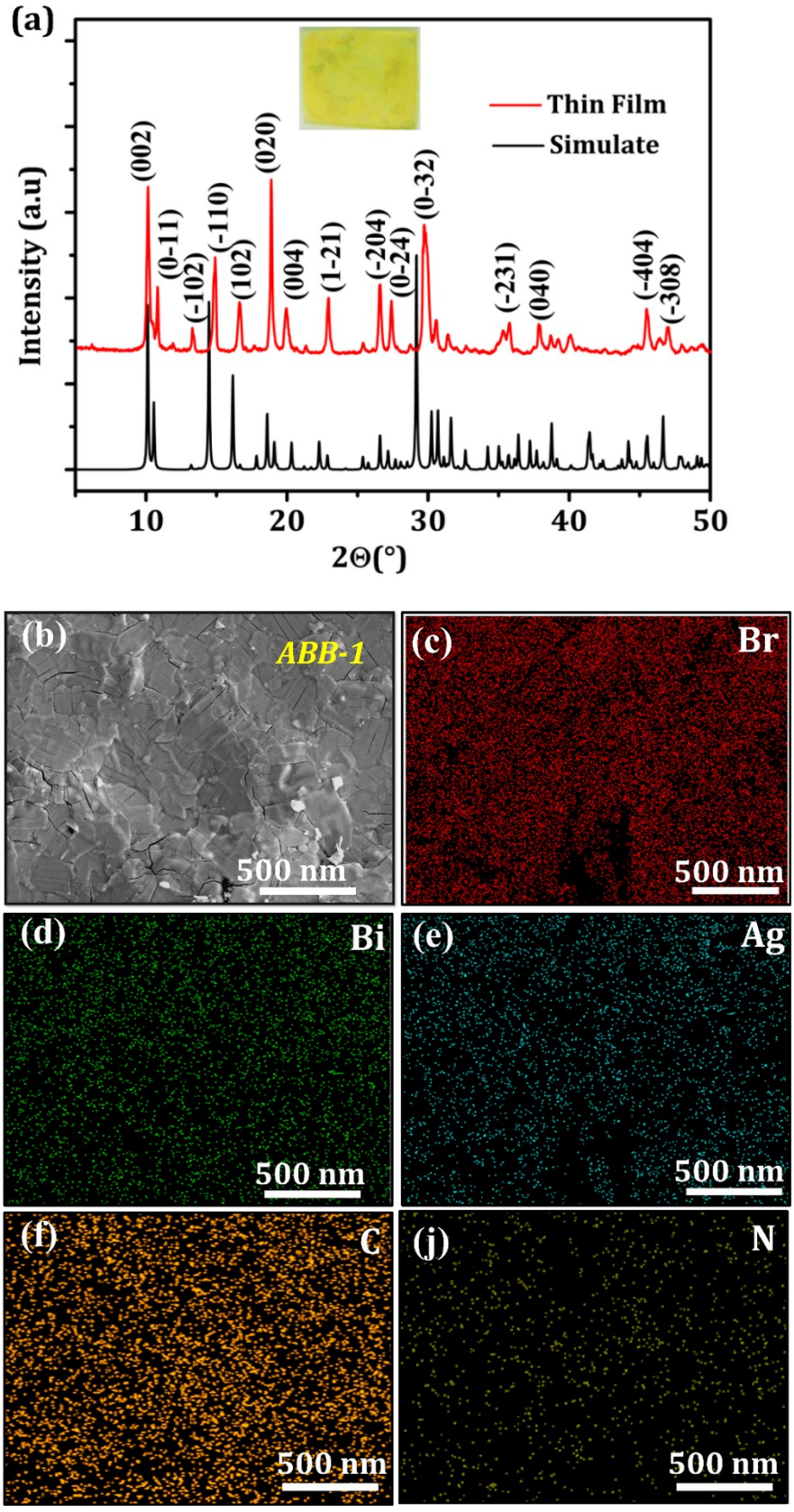

Figure S6. (a) Thin Film XRD patterns for ABB-1, (b-j) SEM and elemental mapping of ABB-1.

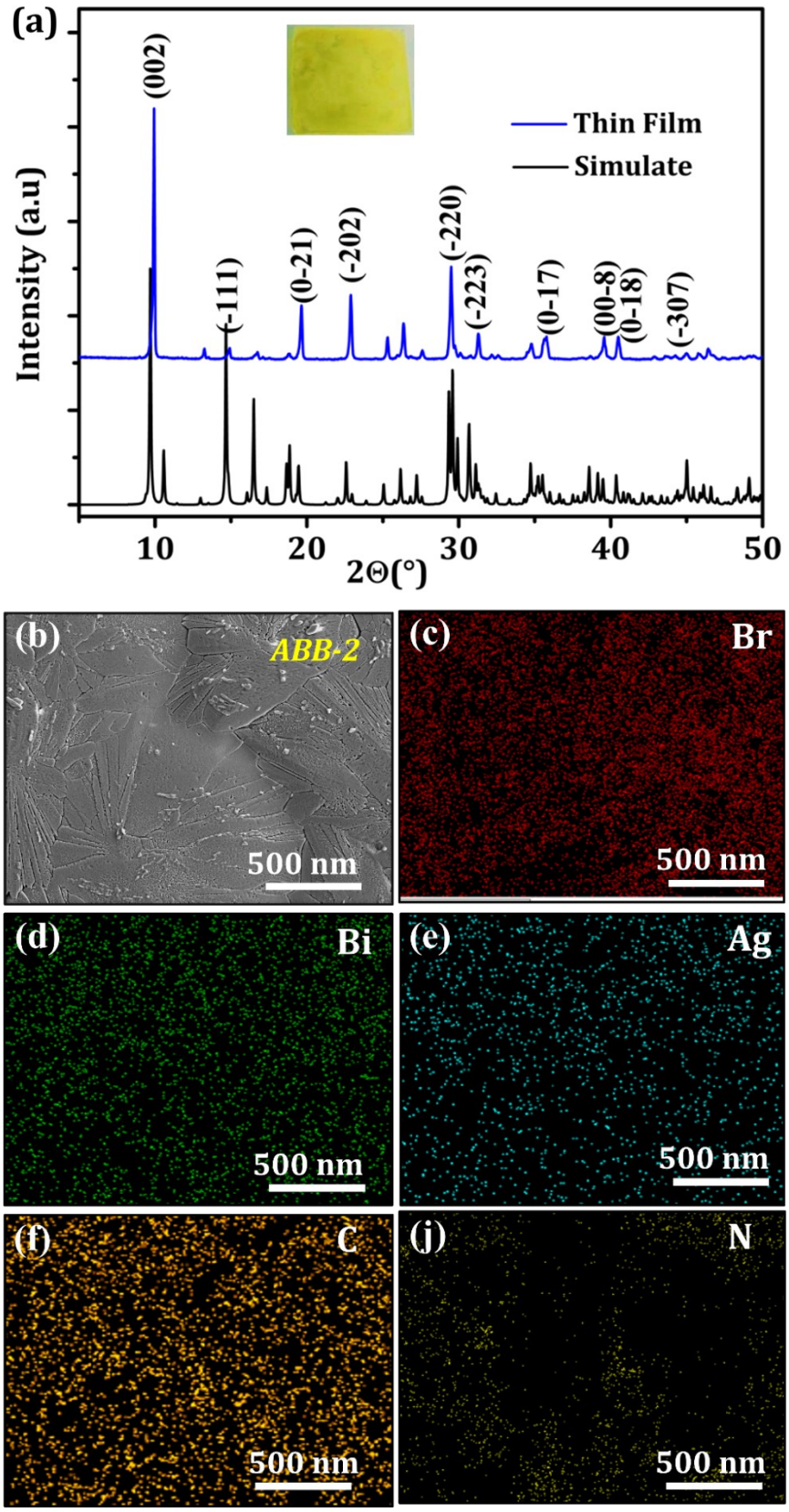

Figure S7. (a) Thin Film XRD patterns for ABB-2, (b-j) SEM and elemental mapping of ABB-2.

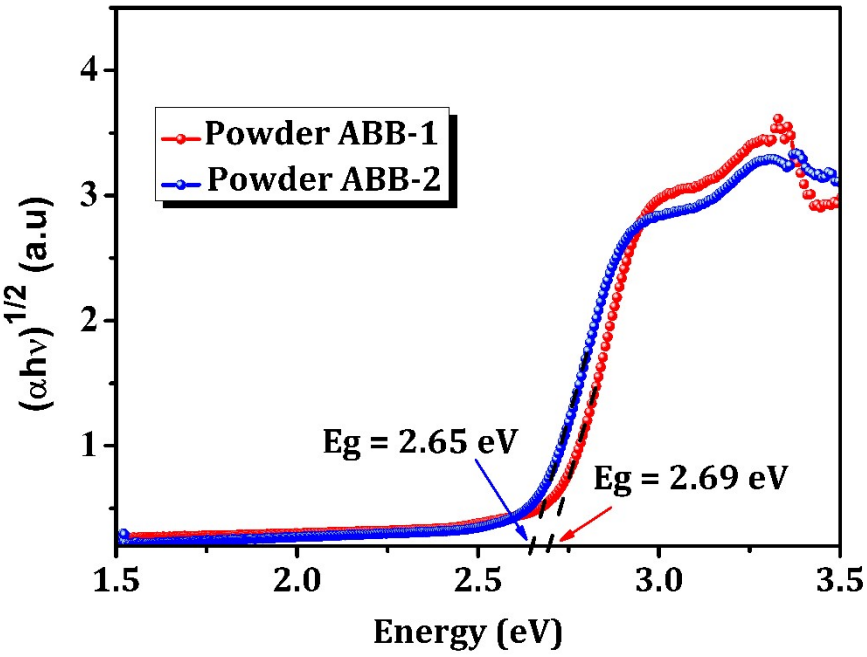

Figure S8. The Tauc Plot for indirect band gap semiconductor for ABB-1 and ABB-2 powders.

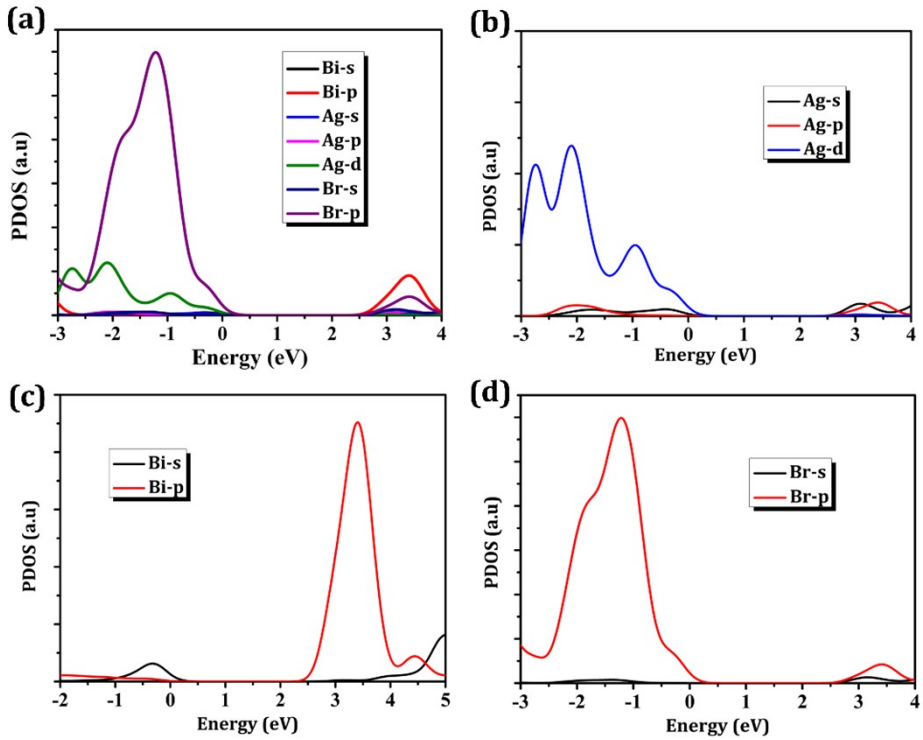

Figure S9. Partial density of states (PDOS) for compound ABB-1 (Inorganic part (a), Ag-s, Ag-p and Ag-d (b), Bi-s and Bi-p (c), and Br-s, Br-p (d)).

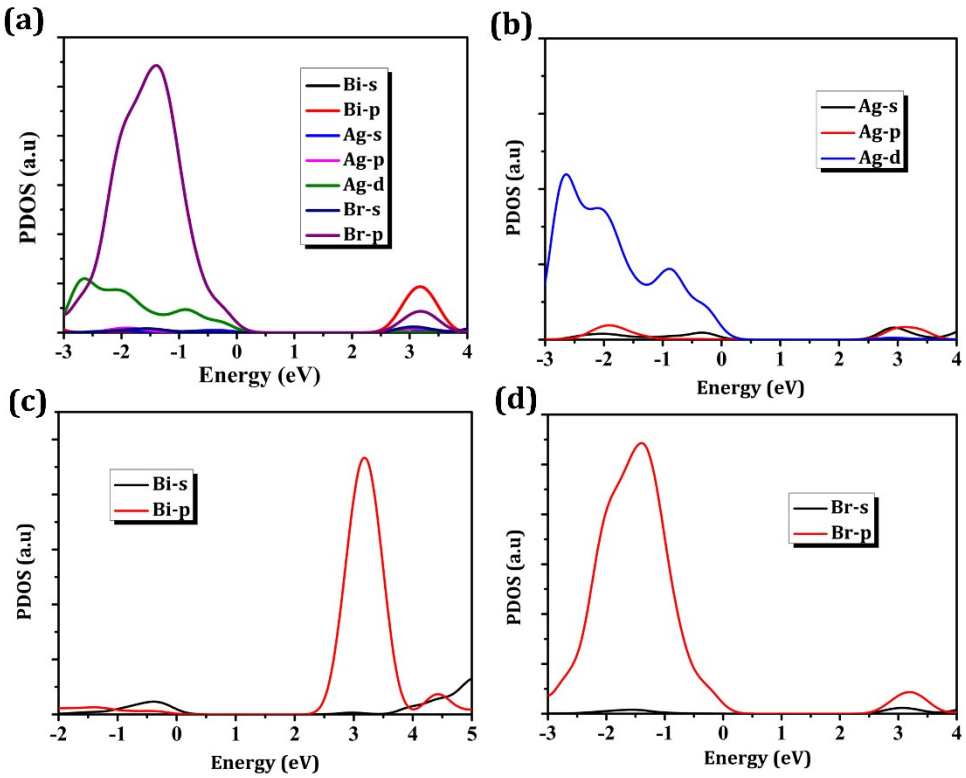

Figure S10. Partial density of states (PDOS) for compound ABB-2 (Inorganic part (a), Ag-s, Ag-p and Ag-d (b), Bi-s and Bi-p (c), and Br-s, Br-p (d)).

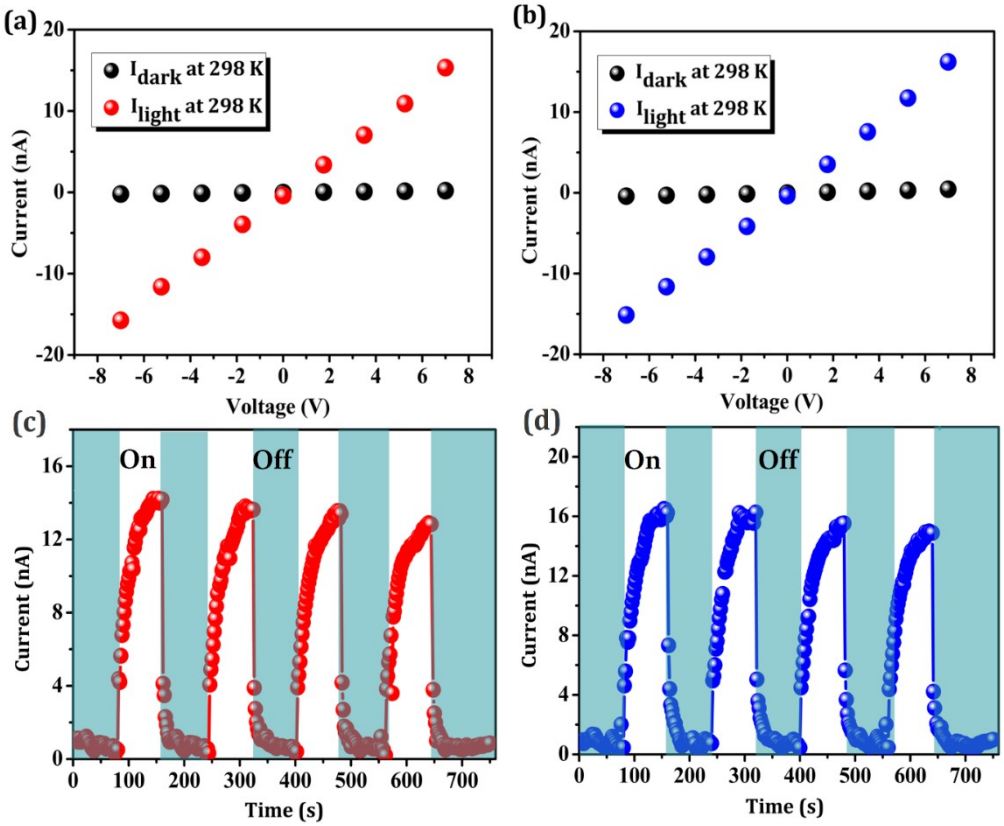

Figure S11. (a, b) *I*–*V* plots for dark and light current of ABB-1 (b) and ABB-2 (b). (c, d) *I*–*t* plots of several irradiation cycles for ABB-1 (c) and ABB-2 (d).

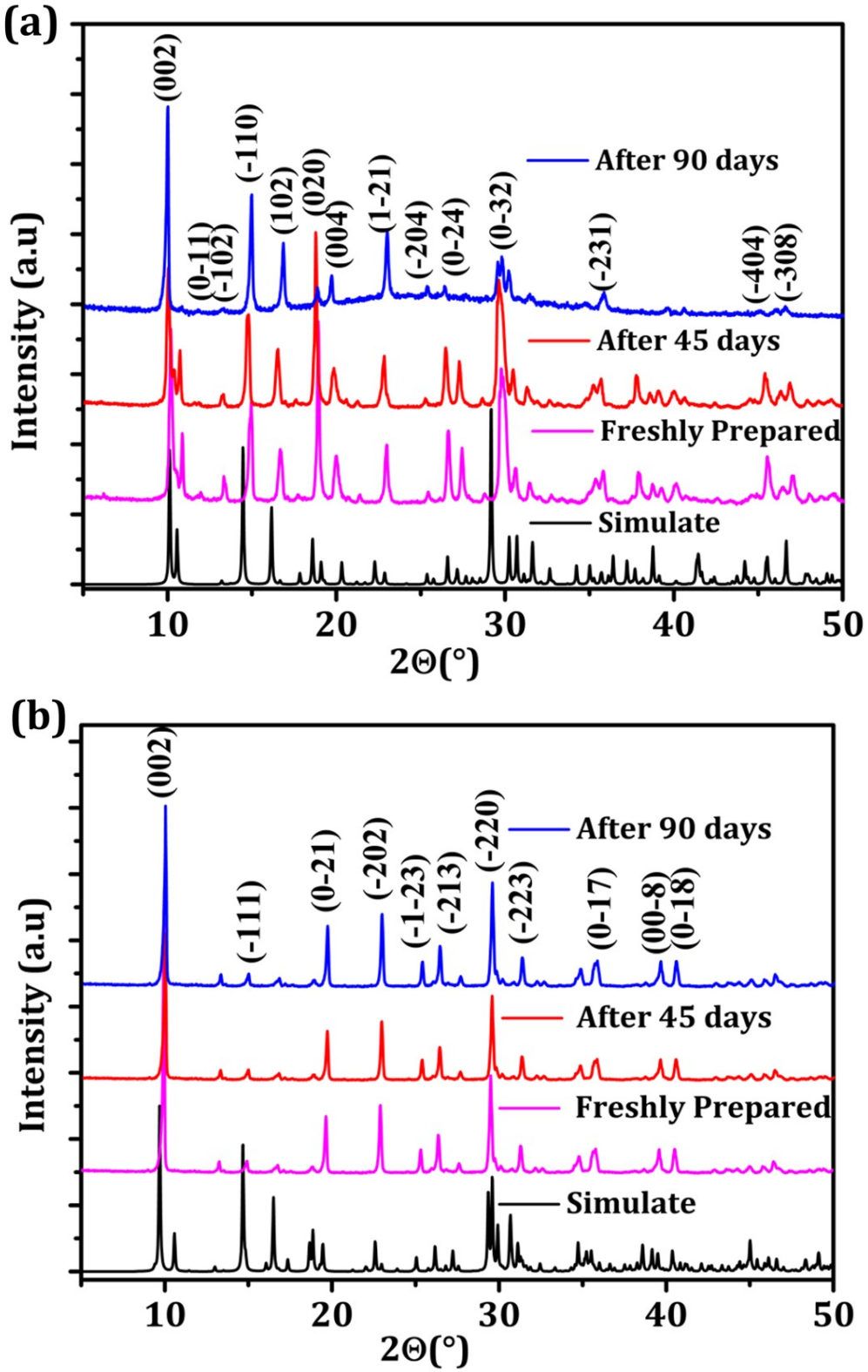

Figure S12. (a) XRD patterns of ABB-1 and ABB-2 films before and after exposure to humidity (55% RH) at different times.

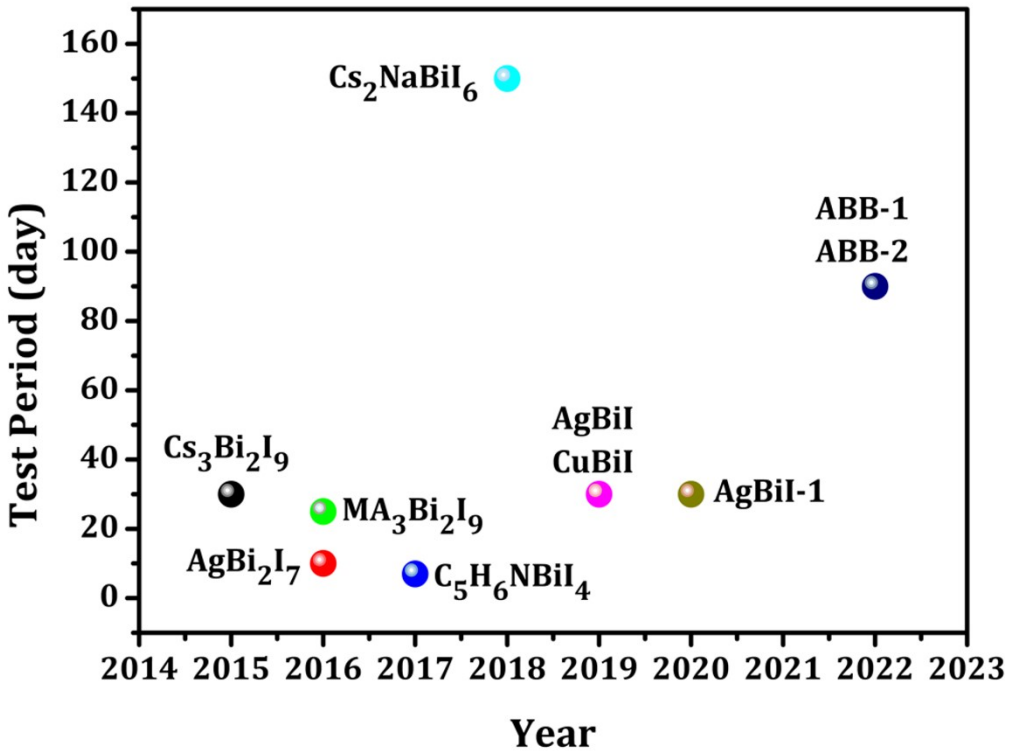

Figure S13. Evolution of the test period of lead-free perovskite material (Where AgBiI: $(C_6H_{16}N_2)_2BiAgI_8{\cdot}H_2O$/ CuBiI: $(C_6H_{16}N_2)_2BiAgI_8{\cdot}0.5H_2O$ and AgBiI-1: $(C_{10}H_{26}N_4)_2BiAgI_8.H_2O$)

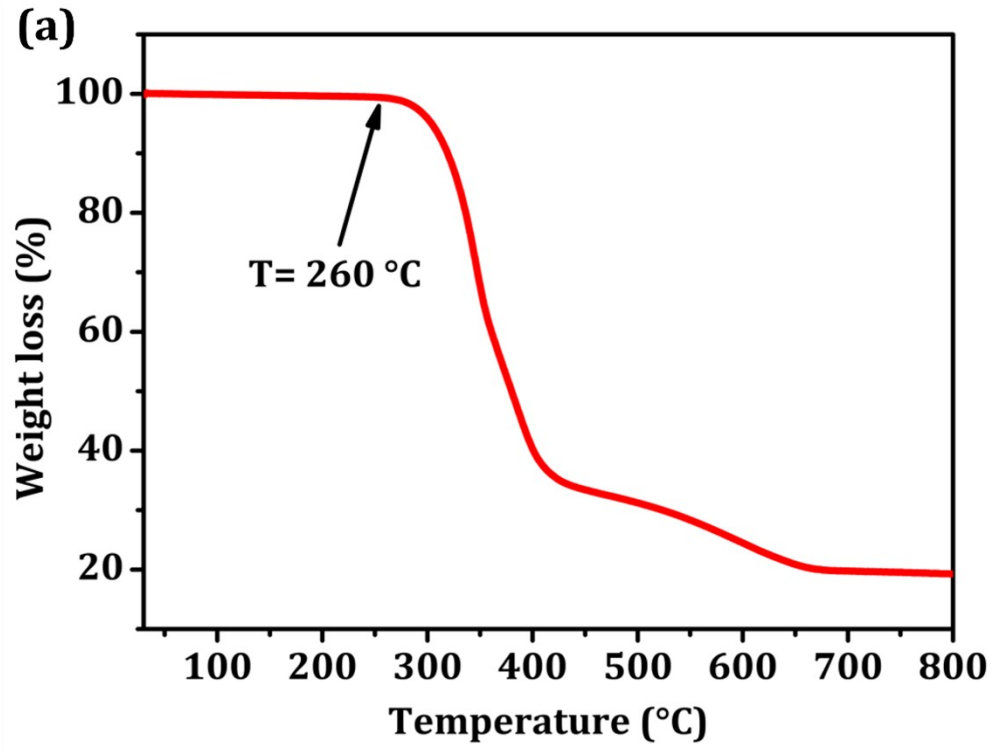

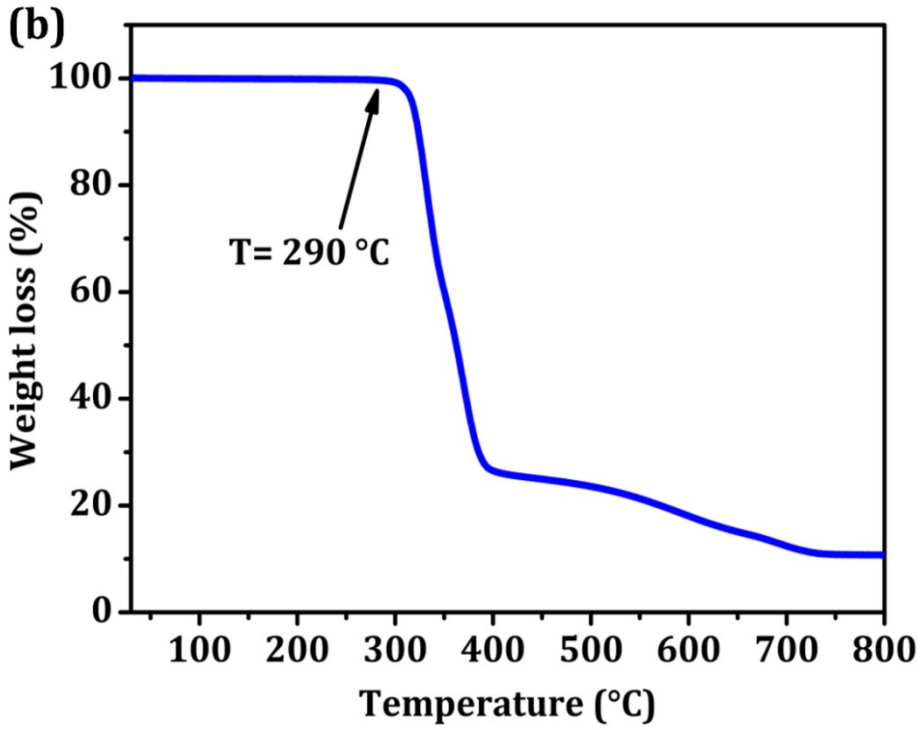

Figure S14. TGA curves of of ABB-1 (a) and ABB-2 (b)

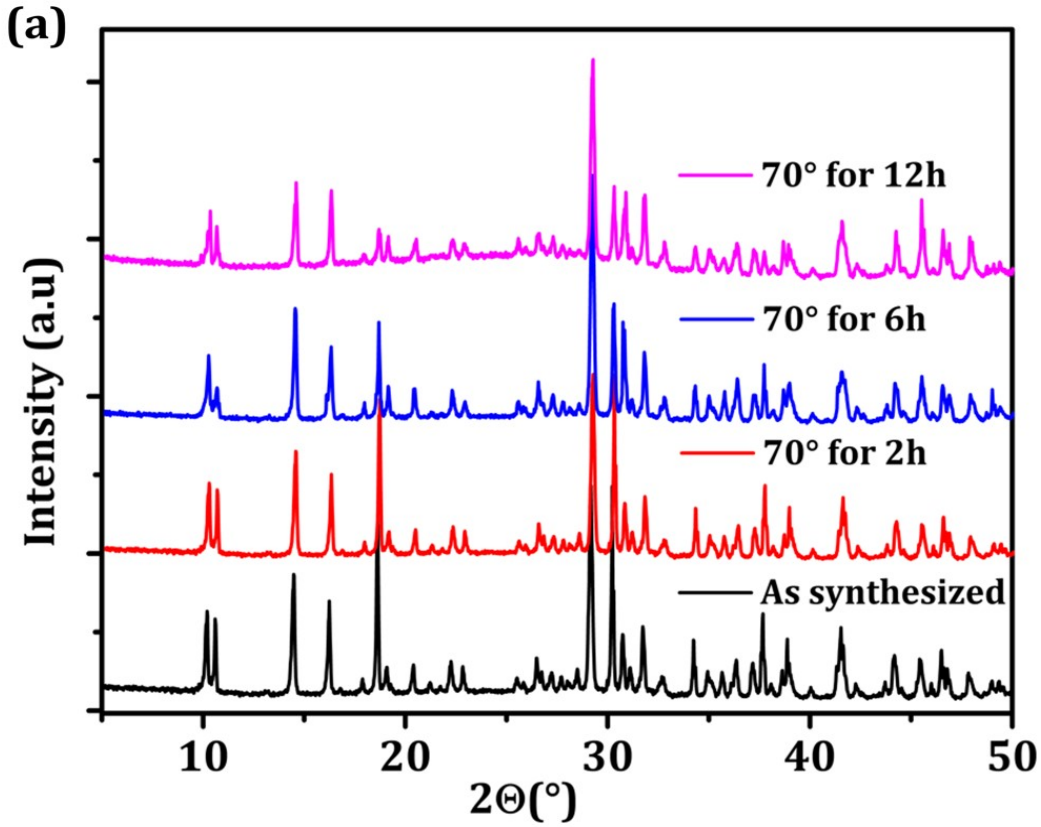

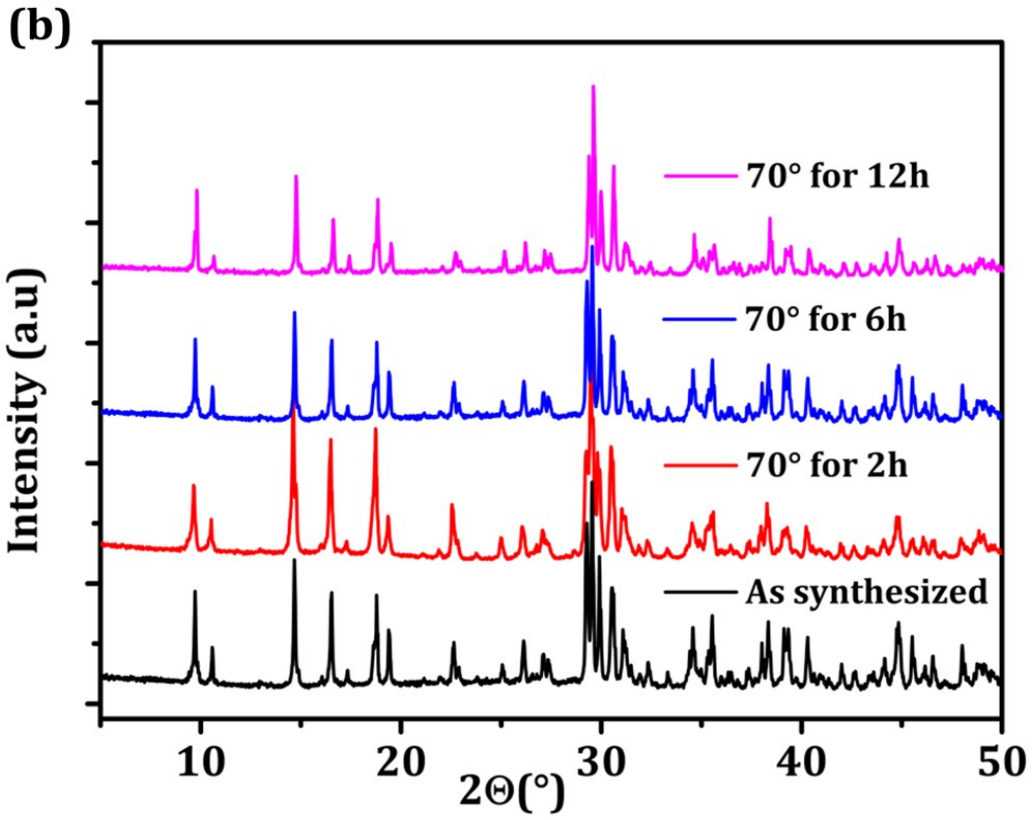

Figure S15. PXRD patterns of the freshly prepared powders of ABB-1 (a) and ABB-2 (b), heated at 70 °C for 2 h, 6h and 12h.

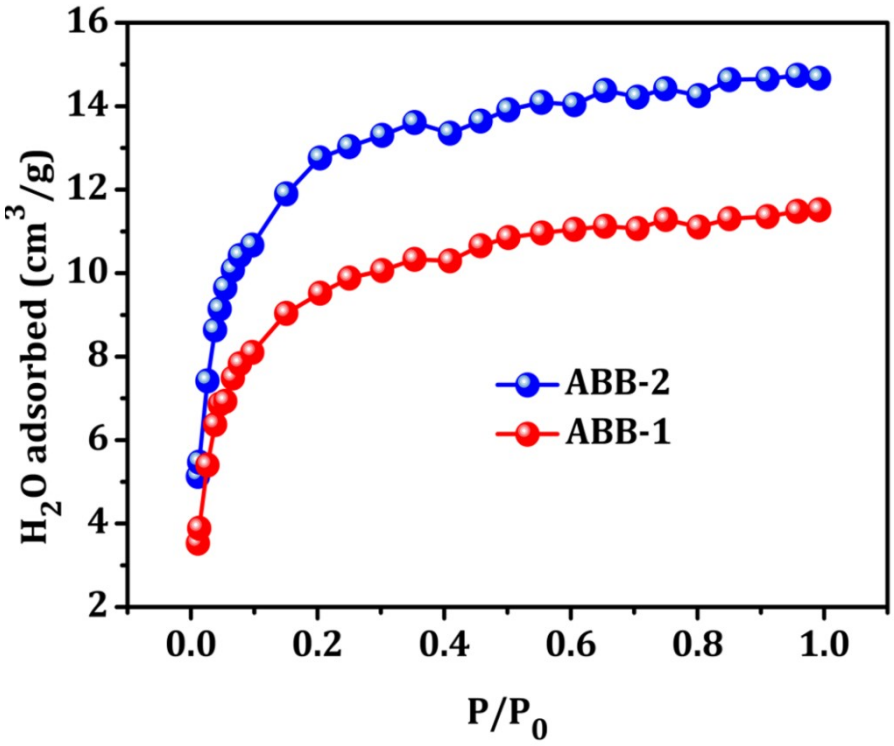

Figure S16. Water vapor adsorption of ABB-1 and ABB-2

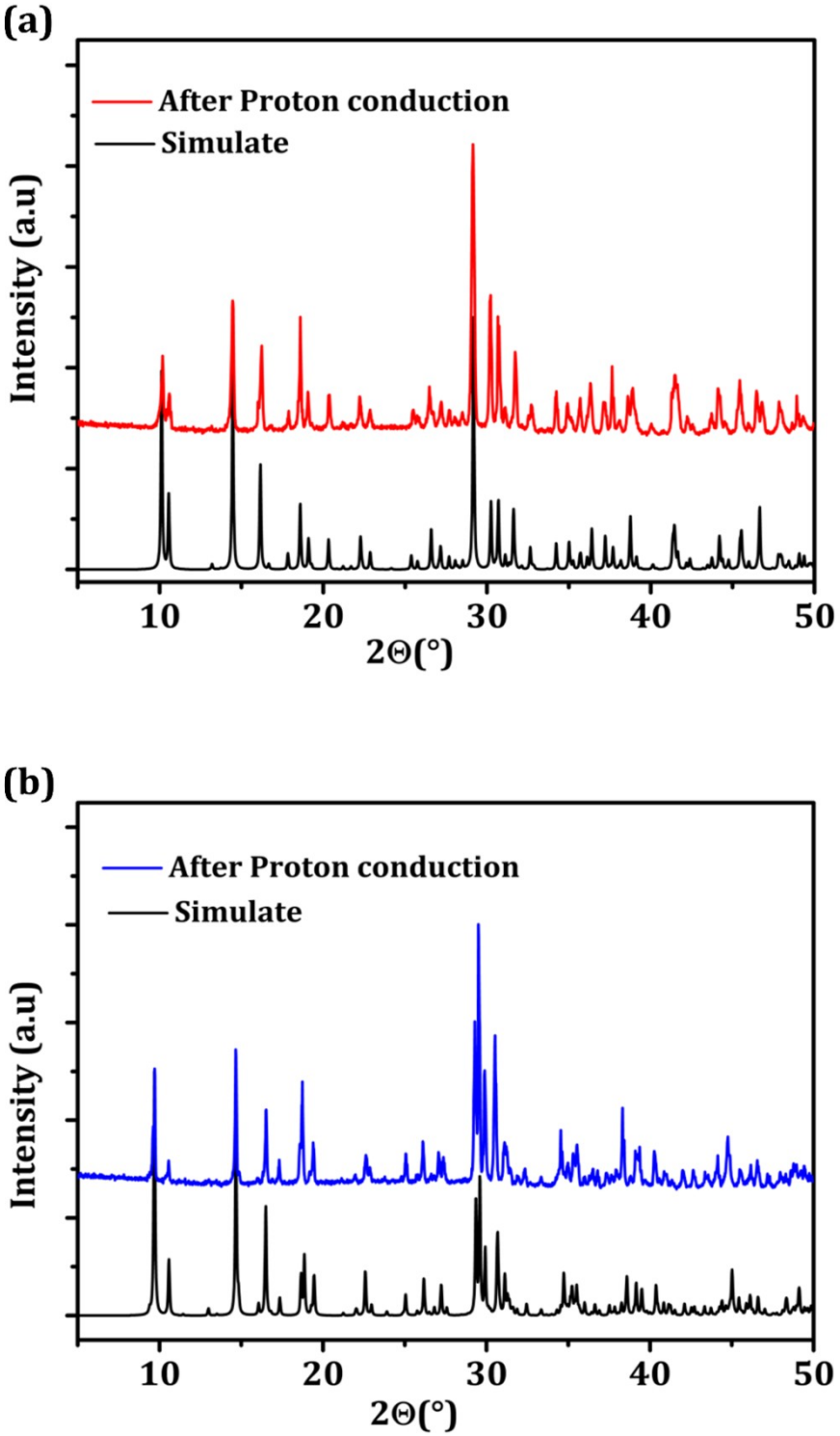

Figure S17. Comparisons of the powder X-ray diffraction (PXRD) patterns of ABB-1 (a) and ABB-2 (b) before and after proton conduction measurements

References

[S1] Sheldrick G. A Short History of Shelx [J]. Acta Crystallographica Section A. **2008**, 64, 112-122.

[S2] F. E. M. O'BRIEN, The Control of Humidity by Saturated Salt Solutions, J. Sci. Instrum. **1948**, 25, 73–76.

[S3] M. D. Segall, J. D. L. Philip, M. J. Probert, C. J. Pickard, P. J. Hasnip, S. J. Clark and M. C. Payne, J. Phys.: Condens. Matter. **2002**, 14, 2717.

[S4] J. Hafner, J. Comput. Chem, **2008**. 29, 2044-2078.

[S5] Perdew J P, Burke K, Ernzerhof M. Generalized Gradient Approximation Made Simple [J]. Physical Review Letter. **1996**, 77, 3865-3868.

[S6] L.-Y. Bi, T.-L. Hu, M.-Q. Li, B.-K. Ling, M. S. Lassoued, Y.-Q. Hu, Z. Wu, G. Zhou and Y.-Z. Zheng, J. Mater. Chem. A. **2020**, 8, 7288–7296.

[S7] L.-Y. Bi, Y.-Q. Hu, M.-Q. Li, T.-L. Hu, H.-L. Zhang, X.-T. Yin, W.-X. Que, M. S. Lassoued and Y.-Z. Zheng, J. Mater. Chem. A. **2019**, 7, 19662–19667.

[S8] W. Zhang, K. Tao, C. Ji, Z. Sun, S. Han, J. Zhang, Z. Wu, and J. Luo, Inorg. Chem, **2018**, 57, 4239−4243.

[S9] M. S. Lassoued, L-Y. Bi, Z. Wu, G. Zhou and Y-Z. Zheng, Mater. Chem. Front, **2021**, 5, 973-978.

[S10] J. K. Pious, A. Katre, C. Muthu, S. Chakraborty, S. Krishna, and C. Vijayakumar, Chem. Mater, **2019**, 31, 1941−1945.

[S11] L-Y. Bi, Y-Q. Hu, M-Q. Li, T-L. Hu, H-L. Zhang, X-T. Yin, W-X. Que, M. S. Lassoued and Y-Z. Zheng, J. Mater. Chem. A, **2019**, 7, 19662-19667.

[S12] Y. Wang, S. Han, Y. Liu, Y. Li, Z. Sun, and J. Luo, Chem Asian J, **2020**, 15, 3350 −3355.

[S13] X. Li, D. Li, Y. Peng, Y. Liu, J. Wang, L. Li, Y. Yao, X. Liu and J. Luo, J. Mater. Chem. C, **2021**, 9, 9499-9504.

[S14] W. Guo, H. Chen, X. Liu, Y. Ma, J. Wang, Y. Liu, S. Han, H. Xu, J. Luo and Z. Sun, Sci. China Mater, **2022**, 65, 179–185.

[S15] B. Zhang, J. Li, M. Pang, Y-S. Wang, M-Z. Liu, and H-M. Zhao, Inorg. Chem, **2022**, 61, 406-413.

[S16] B. W. Park, B. Philippe, X. Zhang, H. Rensmo, G. Boschloo and E. M. Johansson, Adv. Mater. **2015**, 27, 6806–6813

[S17] Y. Kim, Z. Yang, A. Jain, O. Voznyy, G. H. Kim, M. Liu, L. N. Quan, F. P. Garcia de Arquer, R. Comin, J. Z. Fan and E. H. Sargent, Angew. Chem. Int. Ed. **2016**, 55, 9586–9590.

[S18] R. L. Hoye, R. E. Brandt, A. Osherov, V. Stevanovic, S. D. Stranks, M. W. Wilson, H. Kim, A. J. Akey, J. D. Perkins, R. C. Kurchin, J. R. Poindexter, E. N. Wang, M. G. Bawendi, V. Bulovic and T. Buonassisi, Chem. Eur.J. **2016**, 22, 2605-

[S19] T. Li, Y. Hu, C. A. Morrison, W. Wu, H. Han and N. Robertson, Sustainable Energy Fuels. **2017**, 1, 308–316.

[S20] C. Zhang, L. Gao, S. Teo, Z. Guo, Z. Xu, S. Zhao and T. Ma, Sustainable Energy & Fuels. **2018**, 2, 2419–2428

[S21] M. S. Lassoued, L.-Y. Bi, Z. Wu, G. Zhou and Y.-Z. Zheng, J. Mater. Chem. C. **2020**, 8, 5349–5354.

[S22] L-K. Gong, K-Z. Du and X-Y. Huang, Dalton Trans. **2019**, 48, 6690-6694.

[S23] M. J. Wang, X. R. Chen, Y. B. Tong, G. J. Yuan, X. M. Ren and J. L. Liu, Inorg. Chem. **2017**, 56, 9525–9534.

[S24] X. Liang, B. Li, M. H. Wang, J. Wang, R. L. Liu and G. Li. ACS Appl. Mater. Interfaces. **2017**, 9, 25082–25086

[S25] R. Li, S-H. Wang, X-X. Chen, J. Lu, Z-H. Fu, Y. Li, G. Xu, F-K. Zheng, and G-C. Guo, Chem. Mater. **2017**, 29, 2321-2331.

[S26] Z-Q. Shi, N-N. Ji, M-H. Wang, and G. Li, Inorg. Chem. **2020**, 59, 4781–4789.